A distribution-free Max-EWMA scheme for multi-aspect process monitoring with industrial applications

Anan Tang, Amitava Mukherjee, Philippe Castagliola

A Distribution-free Max-EWMA Scheme for Multi-aspect Process Monitoring with Industrial Applications

February 24, 2024

Anan Tang. (Corresponding Author) 1.School of Management, Nanjing University of Posts and Telecommunications, Nanjing, China; 2.Jiangsu-Information Industry Integration Innovation and Emergency Management Research Center, Key Research Base of Philosophy and Social Sciences, Nanjing, China. Emai: tanganan2@sina.com.

Amitava Mukherjee. XLRI-Xavier School of Management, XLRI Jamshedpur, India. Email: amitmukh2@yahoo.co.in.

Philippe Castagliola. Nantes Université & LS2N UMR CNRS 6004, Nantes, France. Email: philippe.castagliola@univ-nantes.fr.

A Distribution-free Max-EWMA Scheme for Multi-aspect Process Monitoring with Industrial Applications

ARTICLE INFO

Keywords:
Ansari-Bradley statistic
Max-EWMA scheme
Median run length
Distribution-free
Savage statistic
Wilcoxon statistic

ABSTRACT

In Statistical Process Monitoring, Distribution-free charting schemes play a vital role in Industry 4.0 for their superior effectiveness compared to parametric methods, especially in cases where the underlying process distribution is not well-defined or poses challenges in estimation. Traditional distribution-free charting schemes focus on surveilling only one process aspect: the location or scale parameter. The past two decades have also witnessed a rapid expansion of research on joint monitoring of the two aspects, location and scale, using combined bi-aspect charting schemes. However, there is a notable scarcity of methods that addressing complex industrial scenarios where multiple parameters (like location, scale, and shape) need simultaneous monitoring with high sensitivity and specificity. Our research is motivated by this challenge, and this paper describes a distribution-free tri-aspect monitoring procedure called the Maximum Exponentially Weighted Moving Average (Max-EWMA) scheme. This scheme can effectively monitor shifts in three process characteristics, encompassing aspects related to process location, scale, and shape parameters. We utilize weighted versions of well-known statistical measures such as the Wilcoxon, Ansari-Bradley, and Savage-type statistics to construct the plotting statistics. An essential feature of our proposed Max-EWMA chart is its robustness under various continuous distributions, ensuring reliable performance in in-control situations. Competing schemes are compared via intensive computing techniques based on Monte Carlo using the Median Run Length metric, which evaluates the effectiveness of the proposed scheme. Finally, our proposed schemes are illustrated with two examples. Some concluding remarks and limitations of the study are noted.

1. Introduction

As one of the most extensively applied graphical techniques in Statistical Process Monitoring (SPM), various charting schemes have been widely used in the manufacturing sector since their inception. See Anwar, Aslam, Zaman and Riaz (2021), Mukherjee and Marozzi (2021), Yan, Grasso, Paynabar and Colosimo (2022), Zhao, Lui, Du, Wang and Shao (2023), Wu, Li, Tsung and Pan (2023), for recent charting applications in manufacturing industries. In recent years, the applications of SPM schemes are no longer confined to the manufacturing domain. To understand its application in healthcare surveillance, we recommend Keshavarz, Asadzadeh and Niaki (2021), Erfanian, Sadeghpour Gildeh and Reza Azarpazhooh (2021), and the references cited there. See also Zhang, He, Zhao and Qu (2021) for applications in monitoring service quality, Wu, Castagliola and Celano (2021) for monitoring French forest fire, Chan, Chong and Mukherjee (2022) for monitoring time spent in Google applications and so forth. SPM schemes are often broadly classified as parametric and nonparametric depending on whether the functional form of the distribution is known or estimable from the Phase-I reference sample or unknown. Traditional parametric SPM schemes commonly assume a priori knowledge of the complete distributional structure of the underlying processes. However, fitting a specific parametric distribution in practice can be challenging when an adequately large reference sample is unavailable. The same is also true if the process characteristic has more complex behaviour. The Nonparametric SPM (NSPM) schemes facilitate process monitoring without distributional assumption. Therefore, NSPM schemes have gained considerable popularity in the past twenty years as they offer advantages in dealing with challenges associated with the parametric approach. These alternative charting schemes have emerged as attractive options when limited data is available, or the data does not conform to specific assumptions about the distribution. To this end, we encourage reading the comprehensive textbook by Qiu (2013). An excellent review by Qiu (2018) is also a must-read for a thorough understanding of various perspectives of NSPM schemes.

A common advantage regarding the nonparametric charting scheme is that its In-Control (IC) robustness remains valid regardless of the actual process distribution. Depending on whether the premise is standard known or unknown, the actual or target values of the parameters of the said distribution may be known (Parameter-K) or unknown

ORCID(s):

(Parameter-U). The partitioning of SPM schemes into Parameter-K and Parameter-U is valid in both the parametric and nonparametric setups. However, noting the focus of the current article is nonparametric, we highlight some vital NSPM schemes under Parameter-K and Parameter-U. In a Parameter-K setup, one may consider NSPM schemes based on the sign and Wilcoxon's signed-rank statistics. See, for example, Abid, Nazir, Riaz and Lin (2017), Castagliola, Tran, Celano and Maravelakis (2020), Alevizakos, Chatterjee and Koukouvinos (2021), Rasheed, Zhang, Arslan, Zaman, Anwar, Abid and Abbasi (2021), Rasheed, Khan, Abiodun, Anwar, Khalaf and Abbasi (2022), Zhang, Rasheed, Khan, Namangale, Anwar and Hamid (2022), Almanjahie, Rasheed, Khan, Anwar and Cheema (2023) and Perdikis, Celano, Psarakis and Castagliola (2023). Likewise, Parameter-U NSPM schemes have also drawn significant attention from researchers recently. When the target parameter is unknown, we often consider designing a monitoring scheme based on the ranks or empirical reference distribution. First, a presumably IC sample is gathered when the process behaviour is supposed to be smooth and fine. The observed sample is subsequently processed through appropriate Phase-I analysis and established as a reference sample. Then, we obtain each Phase-II sample that needs to be monitored sequentially and compare it with the reference sample at each monitoring stage unless some signal is raised. Numerous Parameter-U NSPM schemes are presented to monitor the process location. See, for example, Graham, Mukherjee and Chakraborti (2012), Mukherjee and Sen (2015), Li, Mukherjee, Su and Xie (2016), Graham, Mukherjee and Chakraborti (2017), Malela-Majika and Rapoo (2017) and Malela-Majika (2021). There are also some charting schemes for monitoring the process scale. See, for example, Das and Bhattacharya (2008), Zhou, Zhou and Geng (2016) and Haq (2017).

Most existing NSPM schemes cited in the earlier paragraphs, barring Zhang et al. (2021) and Chan et al. (2022), focus on detecting isolated shifts in either the process location or scale parameter. Consequently, they are referred to as uni-aspect NSPM schemes. These uni-aspect schemes utilize plotting statistics explicitly designed to detect only one aspect of process quality. Nevertheless, practical processes often undergo concurrent shifts in location and scale characteristics. Some studies have suggested using a single combined charting statistic to monitor the location and scale parameters simultaneously to avoid such issues. These charting schemes belong to the class of bi-aspect NSPM schemes that evolved from the early works of Mukherjee and Chakraborti (2012) about a decade ago. They used a quadratic combination of the Wilcoxon Rank Sum (WRS) and the Ansari-Bradley (AB) statistics, known as the Lepage Statistic (LS). Subsequently, the authors introduced a bi-aspect Shewhart-LS scheme for examining process location and scale parameters in a Phase-II Parameter-U setup. Mukherjee and Sen (2018) has extended a new class of Shewhart-LS scheme with the adaptive Gastwirth Score. Recent years have witnessed a growing interest in bi-aspect schemes for joint monitoring of the location and scale parameters. Examples of such research include Mukherjee, Cheng and Gong (2018), Xiang, Gao, Li, Pu and Dou (2019), Chong, Mukherjee and Khoo (2020), Song, Mukherjee and Zhang (2020b), Song, Mukherjee, Marozzi and Zhang (2020a), Chan, Mukherjee, Chong and Lee (2021) and Liang, Mukherjee, Xiang and Xu (2022).

In practical applications, the EWMA- and Cumulative Sum (CUSUM)-type schemes are commonly favoured over the Shewhart-type scheme for detecting more moderate and small shifts. A Shewhart-type scheme may, in fact, be looked upon as a particular case of the EWMA scheme when the smoothing parameter $\lambda = 1$. Interested readers may see Chowdhury, Mukherjee and Chakraborti (2015) and Song et al. (2020a) for more details on the bi-aspect NSPM CUSUM-LS and EWMA-LS schemes. Although the uni-aspect and bi-aspect strategies have gained much attention recently, they do not look at the shape parameter separately. Most bi-aspect schemes are inherently sensitive to a shift in shape parameter and perform excellently in practice. However, following up and detecting a shape shift with bi-aspect schemes are difficult as the constituent plotting statistic does not explicitly consider the shape aspect. In dealing with customer satisfaction, product reliability, or Time-Between-Event (TBE) applications, changes in the process shape often occur frequently. By exploring the literature on nonparametric NSPM schemes, we note a relative dearth of research on the simultaneous monitoring of three process aspects: location, scale and shape. Only recently, Mukherjee, Qiu and Marozzi (2021) proposed a Tri-aspect Shewhart NSPM (TNS) scheme. This scheme employs a combined statistic, calculated as the Euclidean distance of the standardized WRS, AB and Savage-type (SA) statistics from the origin. Tang, Mukherjee and Ma (2023) integrated the TNS design with an CUSUM setup.

In contrast to the Shewhart-type chart, where only the current information is used in the plotting statistics, the EWMA-type chart accumulates more recent observations in each sub-chart statistics, leading to improved process monitoring and enhanced detection of process improvements. See, for example, Abid et al. (2017), Graham et al. (2017), Haq (2017), Tang, Castagliola, Sun and Hu (2019), Chan et al. (2022) and Liang et al. (2022). Particularly, recent studies have extensively demonstrated the effectiveness of the Max-EWMA scheme for monitoring parametric processes. For example, Javaid, Noor-ul Amin and Hanif (2020) investigated the performance of the Max-EWMA scheme with measurement error for monitoring process mean and variance. Noorul-Amin, Javaid, Hanif and Dogu

(2022) further considered the auxiliary information to improve the efficiency of the Max-EWMA chart proposed in Javaid et al. (2020). In their study, Sanusi, Teh and Khoo (2020) proposed a Max-EWMA monitoring chart for the joint monitoring of two variables, time (T) and amplitude (X), where T follows an exponential distribution and X follows a gamma distribution. Subsequently, other pairs of distributions for T and X have been explored in the works of Ali, Akram and Shah (2022) and Talib, Ali and Shah (2022).

However, it is noteworthy that studies specifically focusing on nonparametric Max-EWMA control charts are quite rare. In this paper, we explore the application of a tri-aspect nonparametric Max-EWMA (TNME) monitoring scheme, which utilizes the maximum of three (WRS, AB and SA) robust test statistics to achieve comprehensive monitoring. The proposed TNME scheme outperforms current state-of-the-art methods, with the additional advantage of an easy-to-use signaling identification procedure. The key innovations of this paper have been summarized as follows:

1. This paper combines three well-established nonparametric statistics-Wilcoxon, Ansari-Bradley, and Savage-to create effective plotting statistics for detecting different types of shifts. The use of Max-EWMA strategy on the standardized statistics makes the TNME scheme more sensitive to small and moderate shifts compared to existing charts.
2. This paper provides a convenient follow-up procedure that directly compares the component with the Upper Control Limit (UCL) to identify the signalling cause. This avoids the need for complicated analysis when a signal is observed.
3. This paper provides optimal design methodology for the TNME scheme based on Median Run Length (MRL). Simulation studies and real examples demonstrate the superiority of the proposed TNME scheme over existing methods in detecting various shifts.

This article has been arranged and presented in six sections, including this Introduction. Section 2 introduces the tri-aspect nonparametric Max-EWMA scheme by combining the WRS, AB and SA statistics. The remainder of the article is devoted to outlining the novelty of the proposed procedure. Section 3 describes the implementation and the follow-up procedure. The IC robustness and detection ability of the Out-of-control (OOC) state under different continuous distributions are discussed in Section 4. Two real data sets are presented in Section 5 to show the practical applications of our proposed methodology. Finally, we provide some concluding remarks in Section 6.

2. The tri-aspect nonparametric Max-EWMA chart

Let cumulative distribution function (c.d.f.) F_X of the process characteristic under surveillance be unknown but continuous. We consider a set of independently and identically distributed (iid) historical observations, say $\boldsymbol{X_m} = (X_1, X_2, \ldots, X_m)$ of size m, collected from F_X when process behaviour was apparently stable and IC. Further, suppose that $\boldsymbol{X_m}$ is subsequently established as a reference sample through appropriate Phase-I analysis. A proper Phase-I analysis is very important for the success of Phase-II applications; however, it is a different topic and not the focus area of the current investigation. We refer to Li, Mukherjee and Su (2019), Li, Mukherjee and Marozzi (2020) and Suzuki, Murakami and Mukherjee (2021) for more details on multi-aspect Phase-I applications.

During the online inspection at Phase-II, suppose a test sample $\boldsymbol{Y_{t,n}} = (Y_{t1}, Y_{t2}, \ldots, Y_{tn})$ of size n is observed at the t^{th} stage for $t = 1, 2, \ldots$. Suppose further that the population cdf corresponding to an observation in any test sample be F_Y. Note that F_Y is also supposed to be continuous and unknown. Ideally, as long the process is in IC, we expect the identity $F_X \overset{\text{d}}{=} F_Y$ to hold in all respect. We consider a versatile location-scale-shape family of alternatives introduced by Kössler and Mukherjee (2020). The versatile alternative combines the traditional location-scale alternatives used in bi-aspect charting schemes and the Lehmann alternative corresponding to the shape, which is heavily used in lifetime and reliability testing. The model is given by:

$$F_Y(x) = \left[F_X\left(\frac{x-\delta}{e^{\epsilon}}\right)\right]^{e^{\varrho}}, \quad (\delta, \xi, \varrho) \in \mathbb{R}^3, \tag{1}$$

where $\delta, \epsilon, \varrho$, respectively, represent the location, scale and shape parameters. The notation $\mathbb{R}$ stands for the real line, and $\mathbb{R}^3$ is the corresponding three-dimensional real plane. Following Mukherjee et al. (2021), (1) may be written alternatively as:

$$F_Y(x) = \left[F_X\left(\frac{x-\delta}{\epsilon'}\right)\right]^{\varrho'}, \quad \delta \in \mathbb{R}, \epsilon' \in \mathbb{R}^+, \varrho' \in \mathbb{R}^+, \tag{2}$$

where ϵ' and ϱ' are the reparameterized scale and shape parameters. Here $\mathbb{R}^+$ indicates the positive half of the real line. It immediately follows that the probability density function (p.d.f.) of F_Y is

$$f_Y(x) = \frac{\varrho'}{\epsilon'} f_X\left(\frac{x-\delta}{\epsilon'}\right)\left[F_X\left(\frac{x-\delta}{\epsilon'}\right)\right]^{\varrho'-1}, \quad \delta \in \mathbb{R}, \epsilon' \in \mathbb{R}^+, \varrho' \in \mathbb{R}^+. \tag{3}$$

This alternative includes both isolated and mixed types of shifts as flexible options. All embedded hypotheses in the corresponding two-sample comparison studies can be outlined as follows:

- The IC state corresponds to $H_0 : [\delta = 0, \epsilon' = 1, \varrho' = 1]$;
- The pure location shift corresponds to $H_1 : [\delta \neq 0, \epsilon' = 1, \varrho' = 1]$;
- The pure scale shift corresponds to $H_2 : [\delta = 0, \epsilon' \neq 1, \varrho' = 1]$;
- The pure shape shift corresponds to $H_3 : [\delta = 0, \epsilon' = 1, \varrho' \neq 1]$;
- The classical location-scale alternative is a particular case and corresponds to $H_4 : [\delta \neq 0, \epsilon' \neq 1, \varrho' = 1]$;
- The joint location-shape shift is characterised by $H_5 : [\delta \neq 0, \epsilon' = 1, \varrho' \neq 1]$;
- The joint scale-shape shift is characterised by $H_6 : [\delta = 0, \epsilon' \neq 1, \varrho' \neq 1]$;
- The versatile location-scale-shape shift is characterised by $H_7 : [\delta \neq 0, \epsilon' \neq 1, \varrho' \neq 1]$.

At the t^{th} stage, a pooled sample of size $N = m + n$, comprising the m reference sample and the n test sample, is obtained. We then propose the design of a new tri-aspect nonparametric Max-EWMA plotting statistic using three constituent rank statistics, namely, WRS for location, AB for scale and SA for Lehmann alternative involving shape. Let I_i be an indicator variable such that

$$I_i = \begin{cases} 1 & \text{if the } i^{th} \text{ order statistic of the pooled sample belongs to } \boldsymbol{Y_{t,n}}, \\ 0 & \text{otherwise.} \end{cases}$$

The WRS statistic is given as follows:

$$Z_{W,t} = \sum_{i=1}^{N} i I_i, \tag{4}$$

The AB statistic is given as follows:

$$Z_{A,t} = \sum_{i=1}^{N} \left\{ \left| i - \left(\frac{N+1}{2}\right) \right| I_i \right\}. \tag{5}$$

The detection efficacy of the $Z_{W,t}$ statistic for a shift in δ suffers when there is a shift in ϵ'. Similarly, the power of the $Z_{A,t}$ statistic also suffers when a shift in δ is present. The well-known phenomenon was the instrumental motivation behind the bi-aspect Lepage statistic, denoted as L_t, combining the WRS and AB statistics. The L_t statistic is defined by

$$L_t = \left(\frac{Z_{W,t} - \mu_W}{\sigma_W}\right)^2 + \left(\frac{Z_{A,t} - \mu_A}{\sigma_A}\right)^2 = W_t^2 + A_t^2, \tag{6}$$

where

$$\mu_W = E(Z_{W,t}|\text{IC}) = \frac{n(N+1)}{2}, \tag{7}$$

$$\sigma_W^2 = Var(Z_{W,t}|\text{IC}) = \frac{mn(N+1)}{12}; \tag{8}$$

$$\mu_A = E(Z_{A,t}|\text{IC}) = \begin{cases} \frac{n(N^2-1)}{4N} & \text{if } N \text{ is odd} \\ \frac{nN}{4} & \text{if } N \text{ is even,} \end{cases} \tag{9}$$

$$\sigma_A^2 = Var(Z_{A,t}|\text{IC}) = \begin{cases} \frac{mn(N+1)(N^2+3)}{48N^2} & \text{if } N \text{ is odd} \\ \frac{mn(N^2-4)}{48(N-1)} & \text{if } N \text{ is even.} \end{cases} \tag{10}$$

Further, the SA test statistic is given as follows:

$$Z_{S,t} = \sum_{i=1}^{N} \left(\sum_{j=N-i+1}^{N} \frac{1}{j} - 1 \right) I_i. \tag{11}$$

A standardized SA statistic may be realised as follows:

$$S_t^2 = \left(\frac{Z_{S,t} - \mu_S}{\sigma_S} \right)^2, \tag{12}$$

where

$$\mu_S = E(Z_{S,t}|\text{IC}) = 0, \tag{13}$$

$$\sigma_S^2 = Var(Z_{S,t}|\text{IC}) = \frac{mn}{N-1} \left(1 - \frac{1}{N} \sum_{j=1}^{N} \frac{1}{j} \right). \tag{14}$$

It goes without saying that W_t and A_t are linearly independent, while S_t is not independent of W_t and A_t. Based on the above three statistics, three EWMA statistics may designed as follows:

$$Q_{W,t} = \lambda W_t^2 + (1-\lambda) Q_{W,t-1}, \tag{15}$$

$$Q_{A,t} = \lambda A_t^2 + (1-\lambda) Q_{A,t-1}, \tag{16}$$

$$Q_{S,t} = \lambda S_t^2 + (1-\lambda) Q_{S,t-1}, \tag{17}$$

where $Q_{W,0} = E(W_t^2|\text{IC}) = 1$, $Q_{A,0} = E(A_t^2|\text{IC}) = 1$ and $Q_{S,0} = E(S_t^2|\text{IC}) = 1$ are respectively the starting values and $0 < \lambda \leq 1$ is a smoothing constant. Finally, a tri-aspect nonparametric Max-EWMA scheme, refer to as TNME scheme, combining $Q_{W,t}$, $Q_{A,t}$ and $Q_{S,t}$, is computed as

$$M_t = \max(Q_{W,t}, Q_{A,t}, Q_{S,t}). \tag{18}$$

From the theory of linear rank statistics, it is well-known that $Q_{W,t}$, $Q_{A,t}$, and $Q_{S,t}$ are expected to be higher than 1 when the null hypothesis corresponding to the particular parameter is violated. We always expect an upward shift in one or more of $Q_{W,t}$, $Q_{A,t}$, and $Q_{S,t}$, notwithstanding the direction of shifts. Consequently, the plotting M_t statistic would be expected to be larger in an OOC situation. Therefore, the TNME scheme only has an UCL. An OOC signal will be triggered if the value of M_t exceeds UCL. For a Max-EWMA scheme, no additional charting parameter is necessary for its follow-up procedure. The details of the implementation steps and simple post-signal follow-up rule are given in the following section.

3. Implementation and charting design

Figure 1 outlines the step-by-step implementation procedure of the proposed Max-EWMA type TNME scheme for tri-aspect surveillance. Construction of the TNME procedure can be described as follows:

1. To conduct a Phase-I analysis, initially gather a randomly selected reference batch $\boldsymbol{X_m} = (X_1, X_2, \ldots, X_m)$ with m elements from a process confirmed to be IC using a suitable Phase-I technique. Although it is not the focus of this study, an distribution-free approach, essential for identifying an IC reference sample and confirming the IC status, is detailed in Capizzi and Masarotto (2017).

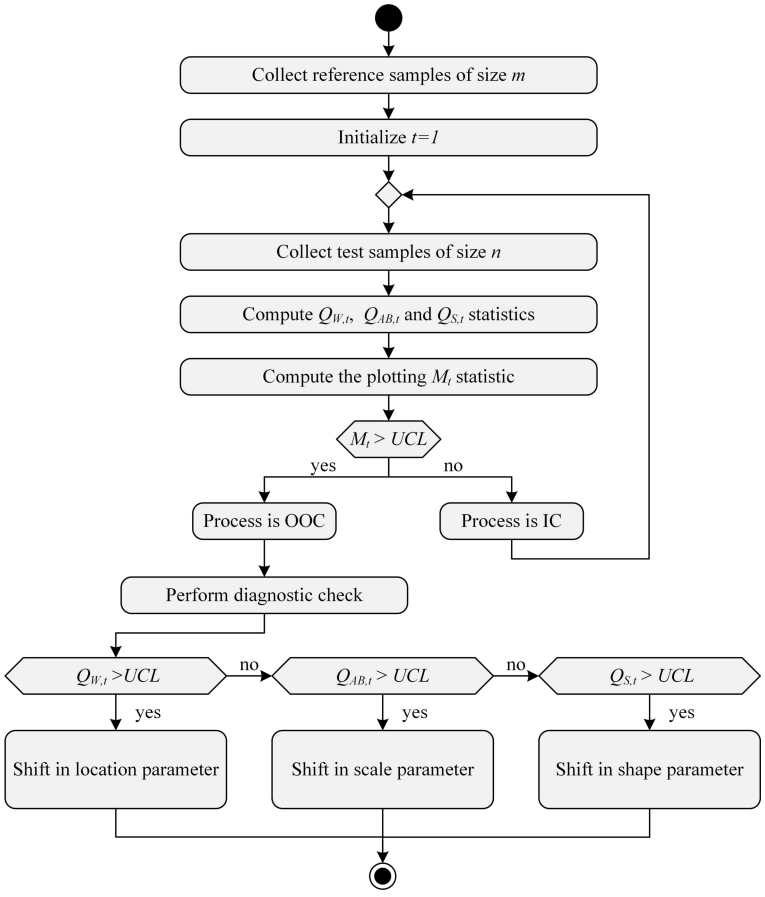

Figure 1: Implementation of the proposed TNME chart.

2. During the online inspection at Phase-II, collect a test sample $\boldsymbol{Y_{t,n}} = (Y_{t1}, Y_{t2}, \ldots, Y_{tn})$ of size n at the t^{th} stage.
3. Compute the standardized statistics W_t^2, A_t^2 and S_t^2 for $t = 1, 2, \ldots$.
4. Calculate the EWMA statistics $Q_{W,t}$, $Q_{A,t}$ and $Q_{S,t}$ and the plotting statistic $M_t = \max(Q_{W,t}, Q_{A,t}, Q_{S,t})$ of the TNME scheme.
5. Plot M_t against the specified UCL. If $M_t \leq$ UCL, the process is determined to be IC, monitoring continues. It is advised to collect and evaluate the subsequent test samples, as in Step 2. Otherwise, it indicates a potential shift in the process, prompting a follow-up as described in Step 6 for an assignable cause.
6. Follow up: The TNME scheme is straightforward to implement since it does require no additional charting parameters for its follow-up procedure. If an OOC situation is detected, any component $Q_{W,t}$, $Q_{A,t}$ and $Q_{S,t}$ exceeding the UCL can be considered as the primary cause of the deviation in the signal. It's important to note that in this context, the UCL value is the same as previously defined. Therefore, there is no need to introduce additional parameters.

3.1. Determination of UCL

The proposed charting scheme and its merits depend on the two design parameters, UCL and the smoothing parameter λ. Following standard practices, we recommend the IC run-length properties to determine the UCL values for a given (m, n, λ). The run length (RL) refers to the number of subgroup samples drawn from the beginning of Phase-II monitoring until the first alarm is issued, and its average value is called the Average Run Length (ARL). Traditionally, practitioners fix a target IC ARL (ARL_0) and aim to search for the optimal OOC ARL (ARL_1). Nevertheless, the use of the ARL has recently been criticised. In most cases, the RL distribution is substantially skewed, and its form also changes according to the shift magnitudes. Also, the existence of theoretical expectation of the RL variable with small

m and λ is questionable in various Phase-II distribution-free monitoring schemes. See Chakraborti, Van der Laan and Van de Wiel (2004).

On the contrary, the MRL is less affected by the skewness, and it can provide a measure of the central tendency of the RL distribution. Also, the median of the RL variable always exists. The MRL performance measure has also been used by You, Khoo, Castagliola and Qu (2016), Teoh, Chong, Khoo, Castagliola and Yeong (2017), Teoh, Lim, Khoo, Chong and Yeong (2018), Tang et al. (2019), Mukherjee and Marozzi (2021) and Chong, Tan, Khoo, Teoh and Castagliola (2022), among others. To this end, we set the target IC MRL value (MRL_0) to 250 in this paper, meaning that the TNME chart will trigger a first OOC alarm at or before the 250th test sample 50% of the time. Choosing charting parameters (UCL, λ) often involves two steps: First, finding the combinations of (UCL, λ) that yield the desired IC MRL value (e.g. $\text{MRL}_0 = C$). The step involves using a dichotomy method to estimate the appropriate UCL value for a given m, n, λ and C. In the second step, optimal λ is chosen amongst various (UCL, λ) combinations, the one that offers the best overall performance for detecting shifts of various sizes. Next, we describe the pseudocode for determining the UCL values, considering fixed values of m, n, and λ that result in a nominal IC MRL_0 close to the target value. See Algorithm 1 for the same. It should be noted that the estimated UCL can be applied to any continuous distribution since the TNME charting scheme is distribution-free. The 10^6 replications in Matlab for calculating UCL should be enough to obtain reliable approximations.

Algorithm 1 Search the UCL

Define m, n, λ and C
$min \leftarrow 1$
$max \leftarrow$ a large value, e.g. 20
$mid \leftarrow 1$
UCL $\leftarrow 1$
while $min < max$ and UCL $= 1$
  do $mid \leftarrow (min + max)/2$
    if $|(\text{MRL}_0(mid, \lambda, m, n) - C)/C| \leq 0.01$
      then UCL $\leftarrow mid$
    else if $|(\text{MRL}_0(mid, \lambda, m, n) - C)/C| > 0.01$
      then $max \leftarrow mid$
    else $min \leftarrow mid$
return UCL

3.2. Problem with the choice of λ

Selecting an appropriate λ is essential to obtain optimal performance of the charting schemes. The choice of λ is tricky. When MRL_0 is prefixed, and the shift size is known, the optimal λ is the TNME(λ) scheme one that offers the smallest OOC MRL ($\text{MRL}_{1,\lambda}$). The same idea may be extended to compare various monitoring schemes for a given shift. From our experience, we know that a typical recommendation is to choose a small λ, say equal to 0.05 to 0.1, for small shifts and larger λ for relatively larger shifts when charts are designed using prefixed ARL_0 or MRL_0. The same logic is applicable in the current context. However, the unknown shift size is the major challenge in the current context. In practice, shift size is often unknown; therefore, optimal λ for a given shift may not be optimal in another shift situation. Since possible shift size is unknown at the very outset, choosing a λ which returns good overall performance for a class of shifts using specific suitable metrics for measuring overall performance is essential.

In addition to using MRL as a performance measure, Han and Tsung (2006) propose a Relative Median Index (RMI) for evaluating the ARL performance of a control chart over a range of change magnitudes. In this paper, we consider using the RMI based on the MRL to explore charting schemes' overall performance. The general index RMI for detecting a whole range of shifts is given by

$$\text{RMI}(\text{UCL}, \lambda) = \int_{-\infty}^{+\infty} \int_{0}^{+\infty} \int_{0}^{+\infty} \left(\frac{\text{MRL}(\text{UCL}, \lambda, \delta, \epsilon', \varrho')}{\text{MRL}^{\text{opt}}(\delta, \epsilon', \varrho')} \right) d(\delta) d(\epsilon') d(\varrho'), \tag{19}$$

where $\text{MRL}^{\text{opt}}(\delta, \epsilon', \varrho')$ denotes the minimum MRL_1 value of all charts compared for detecting $(\delta, \epsilon', \varrho')$. Given the challenges in estimating the exact shape of the parameters $(\delta, \epsilon', \varrho')$, we assumed uniform distributions for δ, ϵ', ϱ', respectively. (19) may be written alternatively as:

$$\text{RMI}(\text{UCL}, \lambda) = \frac{1}{K \times P \times Q} \sum_{k=1}^{K} \sum_{p=1}^{P} \sum_{q=1}^{Q} \left(\frac{\text{MRL}(\text{UCL}, \lambda, \delta^{(k)}, \epsilon'^{(p)}, \varrho'^{(q)})}{\text{MRL}^{\text{opt}}(\delta^{(k)}, \epsilon'^{(p)}, \varrho'^{(q)})} \right), \tag{20}$$

where $\text{MRL}(\text{UCL}, \lambda, \delta^{(k)}, \epsilon'^{(p)}, \varrho'^{(q)})$ denotes the MRL for detecting the shift $(\delta^{(k)}, \epsilon'^{(p)}, \varrho'^{(q)})$, and $K \times P \times Q$ is the number of shift combinations considered in the comparison. Therefore, $\text{RMI}(\text{UCL}, \lambda)$ is a relative efficiency measure of the chart (UCL, λ) compared to the best-performing chart. A smaller RMI indicates that the chart (UCL, λ) outperforms others in detecting shifts overall. The subsequent steps outline the procedure for searching the optimal λ value.

1) Set m, n and target $\text{MRL}_0 = C$ values and for a fixed λ, compute corresponding UCL by using Algorithm 1.
2) Generate m IC reference observations from a specific distribution, and generate n test observations at the t^{th} stage from the same distribution but with shift $(\delta, \epsilon', \varrho')$. For each combination of (UCL, λ), compute M_t and compare it with UCL, record $\text{RL} = t$ when the first OOC signal is detected at the t^{th} test sample.
3) Repeat step 2 for 10^6 times and compute MRL_1 value for this shifted process.
4) Consider different shift combinations, compute $\text{RMI}(\text{UCL}, \lambda)$ for a whole range of shifts.
5) Finally, select the optimal combination (UCL, λ) having the smallest RMI value.

4. Simulation studies

In this section, we delve into a comprehensive analysis of various aspects related to control charts. We initiate our exploration by investigating the IC properties of the TNME charting scheme. Subsequently, we shift our focus towards evaluating the influence of parameters m and n on the chart's performance. Moving forward, we delve into the determination of the optimal λ value based on the RMI methodology. To conclude this section, we conduct a thorough OOC comparison, pitting our proposed approach against existing competitors in the field.

4.1. IC properties

In Table 1, we present the UCL values corresponding to all $\lambda \in \{0.05, 0.1, 0.15, 0.2, 0.25, 0.3, 0.35, 0.4, 0.45, 0.5\}$ values when target $\text{MRL}_0 = 250$. It is important to emphasize that our TNME scheme is distribution-free. Therefore, both the determination of UCL and the RL performance analysis in this paper can be easily achieved using Monte Carlo simulations. In order to investigate the IC performance of proposed TNME scheme, along with the standard normal distribution, various heavy-tailed and skewed distributions have been considered. These distributions are: (1) The standard normal distribution N(0, 1); (2) The student's-t distribution T(3); (3) The Logistic distribution L(0, $\sqrt{3}/\pi$); (4) The gamma distribution G(3, 5); (5) The logarithmic normal distribution LN(0, 1); (6) The exponential distribution E(1). In Table 2 When $(\delta = 0, \epsilon' = 1, \varrho' = 1)$, we estimate the P_5, P_{25}, P_{50}, P_{75} and P_{95} percentiles as well as the ARL_0, and the Standard Deviation ARL (SDRL_0) of the IC RL distribution for the target $\text{MRL}_0 = 250$.

Here, we illustrate the IC performance of the TNME scheme using $\lambda = 0.1$ as an example, considering $m \in \{100, 300\}$ for the reference sample size, $n \in \{5, 10\}$ for the test sample size. Notably, the TNME scheme consistently exhibits MRL_0 values close to the target value, irrespective of the process distributions. While there might be minor sampling fluctuations, these MRL_0 values remain within a narrow range of 247 to 253. This observation leads us to conclude that the IC RL distribution and the associated characteristics of the TNME schemes remain robust across all considered continuous distributions. Table 2 also demonstrates that the ARL_0, SDRL_0 and IC the Quartile Deviation of the RL $\left(\text{QDRL}_0 = \frac{P_{75} - P_{25}}{2}\right)$ value decrease with larger m and n. For example, when $(m, n) = (100, 5)$, for monitoring the N(0, 1) distribution, we have $\text{ARL}_0 = 685.36$, $\text{SDRL}_0 = 1197.99$ and $\text{QDRL}_0 = 320.5$. While when $(m, n) = (100, 10)$, we have $\text{ARL}_0 = 678.36$, $\text{SDRL}_0 = 1159.3$ and $\text{QDRL}_0 = 325$, and $\text{ARL}_0 = 472.29$, $\text{SDRL}_0 = 635.75$ and $\text{QDRL}_0 = 247.5$ for $(m, n) = (300, 10)$.

4.2. Effect of parameters m and n

The OOC c.d.f. is, as you may have noticed in (2), $F_Y(x) = \left[F_X\left(\frac{x-\delta}{\epsilon'}\right)\right]^{\varrho'}$. The probability integral transformation indicates that $F_Y(x)$ follows a uniform distribution across the interval [0, 1]. Our approach involves generating samples

Table 1
UCL for the TNME schemes for $m \in \{100, 300\}$, $n \in \{5, 10\}$ and target $\text{MRL}_0 = 250$.

	$(m,n) = (100,5)$	$(m,n) = (100,10)$	$(m,n) = (300,5)$	$(m,n) = (300,10)$
λ	UCL	UCL	UCL	UCL
0.05	1.728	1.721	1.754	1.737
0.1	2.25	2.23	2.335	2.28
0.15	2.741	2.7	2.887	2.792
0.2	3.214	3.153	3.435	3.294
0.25	3.684	3.602	3.994	3.782
0.3	4.149	4.048	4.537	4.282
0.35	4.621	4.492	5.095	4.764
0.4	5.086	4.935	5.634	5.266
0.45	5.549	5.38	6.178	5.754
0.5	6.028	5.815	6.75	6.258

Table 2
The IC RL profiles of the TNME scheme when target $\text{MRL}_0 = 250$, $\lambda = 0.1$.

$(m,n) = (100,5)$							
	P_5	P_{25}	P_{50}	P_{75}	P_{95}	ARL	SDRL
N(0, 1)	15	81	252	722	2879	685.36	1197.99
T(3)	15	80	250	719	2868	685.56	1200.87
L(0, $\sqrt{3}/\pi$)	15	81	249	710	2852	680.71	1200.12
G(3, 5)	15	81	252	721	2865	682.33	1191.03
LN(0, 1)	14	80	250	714	2877	681.82	1194.10
E(1)	14	80	247	714	2833	677.27	1185.22

$(m,n) = (100,10)$							
	P_5	P_{25}	P_{50}	P_{75}	P_{95}	ARL	SDRL
N(0, 1))	15	80	253	730	2848	678.36	1159.30
T(3)	15	79	251	725	2766	667.08	1146.81
L(0, $\sqrt{3}/\pi$)	15	79	250	717	2808	675.37	1172.98
G(3, 5)	15	79	250	721	2782	668.76	1156.30
LN(0, 1)	15	80	251	717	2781	669.28	1155.88
E(1)	15	79	248	727	2810	673.66	1157.20

$(m,n) = (300,5)$							
	P_5	P_{25}	P_{50}	P_{75}	P_{95}	ARL	SDRL
N(0, 1)	17	91	251	615	1896	516.84	780.07
T(3)	17	91	250	609	1917	516.59	781.07
L(0, $\sqrt{3}/\pi$)	17	92	251	609	1896	515.70	775.33
G(3, 5)	17	91	250	613	1914	519.24	788.24
LN(0, 1)	17	92	251	614	1904	517.93	778.97
E(1)	17	92	252	614	1930	520.20	788.02

$(m,n) = (300,10)$							
	P_5	P_{25}	P_{50}	P_{75}	P_{95}	ARL	SDRL
N(0, 1)	18	92	248	587	1687	472.29	653.75
T(3)	18	93	250	591	1714	478.55	664.99
L(0, $\sqrt{3}/\pi$)	17	92	247	588	1692	474.57	660.10
G(3, 5)	18	93	250	592	1686	474.52	656.75
LN(0, 1)	18	92	249	587	1698	475.57	659.09
E(1)	18	92	249	594	1694	478.93	669.59

from the uniform distribution within the range [0, 1], raising them to the power of ϱ'^{-1}, and then applying the quantile function of the corresponding location-scale distribution family with parameters δ and ϵ'. This method effectively generates random samples for the process observations.

Due to space limitations, we have selected the following three typical distributions for comparison and explanation in cases of OOC situations. Our study encompasses two symmetric distributions and one asymmetric distribution:

- The N(0, 1) distribution is a fundamental distribution in statistics, characterized by its symmetry and bell-shaped curve. It's a common reference point for many statistical methods and theories. Its properties are well understood, making it a natural choice for a baseline comparison;
- The T(3) distribution is chosen for its heavier tails compared to the normal distribution. This makes it useful for studying scenarios where extreme values are more common than what the normal distribution predicts. In practical terms, this distribution can better represent real-world data that may have outliers or be slightly skewed.
- The E(1) distribution is an asymmetric distribution and is often used to model time until an event occurs, such as failure times in reliability testing. Its selection is significant because it differs fundamentally from the symmetric properties of the normal and t-distributions, thus providing a contrasting perspective in the study.

In order to explore the influence of m and n on the OOC performance of the proposed TNME chart, we present the MRL_1 values for different scenarios involving $m \in \{100, 300\}$ and $n \in \{5, 10\}$ in Table 3. An interesting finding in the comparative results is the consistent decrease in MRL_1 values as both m and n increase across all control schemes. Furthermore, it's worth highlighting that the enhancement of charting scheme performance is more noticeable with an increase in n. For example, in Table 3, when $m = 100$, $n = 5$, for detecting $(\delta, \epsilon', \varrho') = (0.2, 1.2, 1.2)$ in N(0.5), we have $MRL_1 = 12$ for the TNME ($\lambda = 0.05$) chart, $MRL_1 = 11$ for the TNME ($\lambda = 0.1$) chart, 12 for the TNME ($\lambda = 0.3$) chart and 13 for the TNME ($\lambda = 0.5$) chart. When n increases to 10, for a same $m = 100$ we have $MRL_1 = 8$ for the TNME ($\lambda = 0.05$) chart, $MRL_1 = 7$ for the TNME ($\lambda = 0.1$) chart, 8 for the TNME ($\lambda = 0.3$) chart and 8 for the TNME ($\lambda = 0.5$) chart. But for the increasing of m, this improvement in detecting performance is not as great as n. For example, when $m = 300$ and $n = 5$, for detecting $(\delta, \epsilon', \varrho') = (0.2, 1.2, 1.2)$, we have $MRL_1 = 10$ for the TNME ($\lambda = 0.1$) chart, $MRL_1 = 9$ for the TNME ($\lambda = 0.1$) chart, 11 for the TNME ($\lambda = 0.3$) chart and 11 for the TNME ($\lambda = 0.5$) chart.

4.3. Optimal λ based on RMI

The overall performance based on RMI is investigated within $\lambda \in \{0.05, 0.1, \ldots, 0.5\}$. Our study includes one asymmetric and two symmetric distributions to search the optimal λ over a wide range of shifts. We also have investigated several larger λ and find that the TNME chart with $\lambda > 0.5$ has no advantage for different shift combinations, so we drop these results. We consider location parameters as $\delta \in \{0, 0.1, 0.25, 0.5, 0.75, 1.0, 1.5, 2\}$, and increasing variability is of major concern, and thus, we consider scale parameters as $\epsilon' \in \{1, 1.25.1.5, 1.75, 2\}$. Also, we choose shape parameters as $\varrho' \in \{1, 2, 5, 10\}$. Therefore, we have $8 \times 5 \times 4 = 160$ combinations of $(\delta, \epsilon', \varrho')$. Clearly, the setting $(\delta, \epsilon', \varrho') = (0, 1, 1)$ corresponds to the IC scenario.

The performance of the TNME scheme in detecting a wide array of shifts is showcased in Figure 2, evaluated through the RMI index. For instance, in Figure 1(a) with parameters $m = 100$ and $n = 5$, the TNME chart with $\lambda = 0.3$ (indicated by the "-∘-" line) exhibits the smallest RMI under the N(0, 1) distribution. Similarly, the TNME chart with $\lambda = 0.3$ proves effective in detecting shifts within the T(3) distribution ("-⋄-" line), while the TNME chart with $\lambda = 0.2$ performs optimally under the E(1) distribution ("-□-" line). Additionally, the mean value of the RMI scores is computed across the three distributions, represented by the "-∗-" line. This visualization underscores that the TNME chart with $\lambda = 0.3$ yields the best performance, followed by the TNME scheme with $\lambda = 0.2$, and then with $\lambda = 0.2$.

4.4. Comparison with existing competitors

For assessing our proposed scheme for detecting OOC cases, we facilitate performance comparisons with the EWMA Cramér-von Mises (ECvM) scheme proposed in Zhang, Li and Li (2017), the EWMA-Lepage (EL) scheme proposed in Song et al. (2020a), the tri-aspect nonparametric CUSUM (TNC) scheme proposed in Tang et al. (2023) and the distribution-free chart based on the score test (DFS) scheme proposed in Ding, Li, Tsung and Li (2023). For brevity, in this subsection, our attention is directed towards assessing the detection performance under the $(m, n) = (100, 5)$ scenario.

The CvM statistic in Zhang et al. (2017) is given by:

$$W_{m,n,t} = \frac{mn}{(m+n)^2}\left(\sum_{i=1}^{m}(\hat{F}_X(x_i) - \hat{F}_Y(x_i))^2 + \sum_{j=1}^{n}(\hat{F}_X(y_{tj}) - \hat{F}_Y(y_{tj}))^2\right) \tag{21}$$

where $\hat{F}_X(x) = \frac{1}{m}\sum_{i=1}^{m}\ell(x_i \le x)$ and $\hat{F}_Y(y) = \frac{1}{n}\sum_{j=1}^{n}\ell(y_{tj} \le y)$ represent the empirical cumulative distribution functions (CDFs) based on the m and n observations, respectively. The $\ell(\boldsymbol{B})$ is an indicator variable, taking the value 1 when $\boldsymbol{B}$ is true and 0 otherwise. Notably, Zhang et al. (2017) explored an EWMA approach employing the standardized CvM statistic, which can be highlighted as follows:

$$U_t = \frac{W_{m,n,t} - \mu_{W_{m,n}}}{\sigma_{W_{m,n}}}, \tag{22}$$

$$E_t = \lambda U_t + (1-\lambda)E_{t-1}, \tag{23}$$

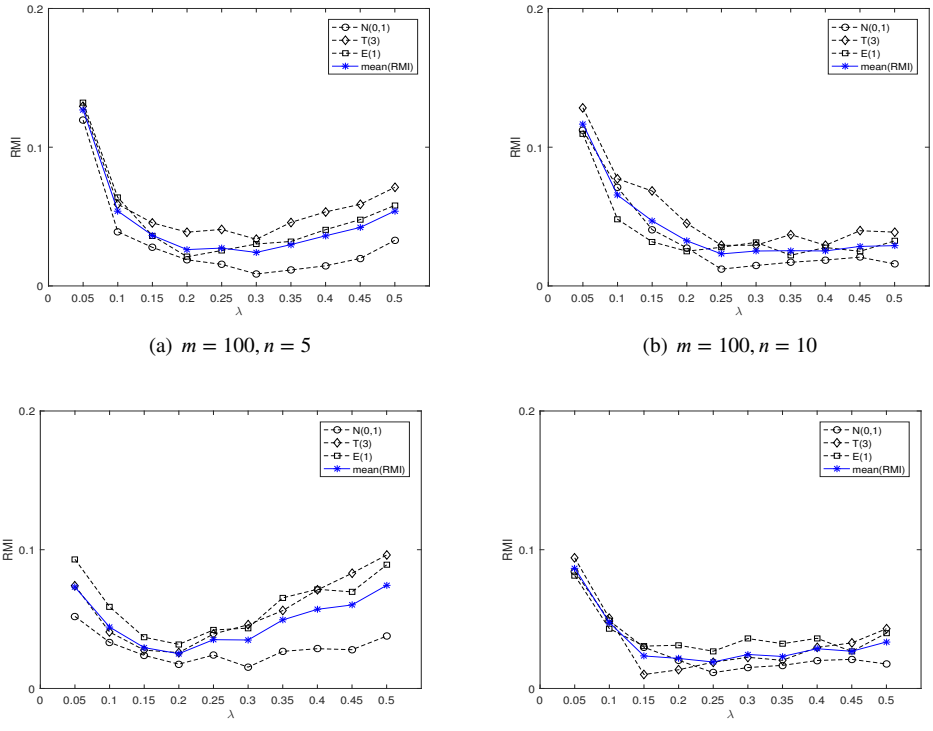

(a) $m = 100, n = 5$ (b) $m = 100, n = 10$

(c) $m = 300, n = 5$ (d) $m = 300, n = 10$

Figure 2: Optimal λ selection based on RMI for the ME-OR scheme when $m \in \{100, 300\}, n \in \{5, 10\}$ and $\text{MRL}_0 = 250$.

with $E_0 = 0$, $\mu_{W_{m,n}} = \frac{m+n+1}{6(m+n)}$ and $\sigma_{W_{m,n}} = \frac{(m+n+1)[(1-\frac{3}{4m})(m+n)^2+(1-m)(m+n)-m]}{45(m+n)^2 n}$.

The EL statistic, as discussed in Song et al. (2020a), constitutes a robust two-sample test designed for a joint location-scale shift hypothesis. This is expressed through equations

$$L_t = W_t^2 + A_t^2, \tag{24}$$
$$Z_t = \lambda L_t + (1-\lambda) Z_{t-1}, \tag{25}$$

with $Z_0 = 2$. When $\lambda = 1$, this EWMA-Lepage scheme coincides with the Shewhart Lepage scheme.

Recently, Tang et al. (2023) introduced a distribution-free CUSUM scheme that relies on the Euclidean distance among the W_t, A_t, and S_t statistics, as follows:

$$T_t = W_t^2 + A_t^2 + S_t^2, \tag{26}$$
$$Q_t = \max\{0, Q_{t-1} + (T_t - 3) - k\}, \tag{27}$$

where $k \geq 0$ is the reference parameter and $Q_0 = 0$.

Ding et al. (2023) introduced a distribution-free EWMA scheme, labelled DFS, for jointly monitoring location and scale. In Ding et al. (2023), they assume the IC c.d.f. F_0 is known or has been accurately estimated. The charting statistic they suggested monitoring is

$$R_t = \frac{1}{n} \theta_t^{\mathrm{T}} \boldsymbol{I}^{-1} \theta_t, \tag{28}$$

where $\theta_t = (1-\lambda)\theta_{t-1} + \lambda\psi_t$, $I = \begin{bmatrix} 1/3 & 0 \\ 0 & (\pi^2+3)/9 \end{bmatrix}$, $\psi_t = \left[\sum_{j=1}^{n} \phi_1(F_0(Y_{tj})), \sum_{j=1}^{n} \phi_2(F_0(Y_{tj}))\right]^{\mathrm{T}}$, $\phi_1(u) = 2u-1$ and $\phi_2(u) = (2u-1)\ln\frac{u}{1-u} - 1$.

Comparing all existing charting schemes with their respective optimal parameters λ (or k) while maintaining a fixed MRL_0 is a more rational approach. Consequently, we explore the optimal values of λ within the range $0.05, 0.1, \ldots, 0.5$ for ECvM, EL, DFS and TNME schemes, encompassing a broad spectrum of shifts. As for the TNC chart, Tang et al. (2023) expressed k in the form $k = h \times SD(T|\mathrm{IC})$, where the k value denotes h times the standard deviation (SD) of T, with an approximate value of $SD(T|\mathrm{IC}) \approx 3.073$. Therefore, when $h \in \{0.05, 0.1, 0.25, 0.5, 0.75, 1, 1.5, 2\}$, we have $k \in \{0.15, 0.31, 0.77, 1.54, 2.30, 3.07, 4.60, 6.15\}$. In Figure 3, we show the RMI performance of the EWMA-CvM, EL and TNC schemes based on different distributions when $m = 100$, $n = 5$ and $\mathrm{MRL}_0 = 250$. Among the considered h values, the TNC scheme with $h = 1$ exhibits favorable overall performance. Similarly, the EWMA-CvM chart with $\lambda = 0.25$, the EL scheme with $\lambda = 0.2$ and the DFS chart with $\lambda = 0.4$ demonstrate the lowest mean(RMI).

Figure 4 illustrates the probability density and cumulative proportion of false alarms for the competing schemes. The x-axis represents the RL with intervals marked up to 5000, while the y-axis shows the cumulative proportion of false alarms, ranging from 0 to 1. It shows that, the curves of all schemes are very close to one another, indicating similar initial performance across the different methods. As RL exceeds 250, the TNME scheme offers a lower cumulative proportion of false alarms than the others. The graph shows that all methods converge towards a cumulative proportion of 1, which is expected for the probability distribution function as RL increases. Around the IC MRL_0 of 250, almost all schemes have a type-I error probability of approximately 0.001.

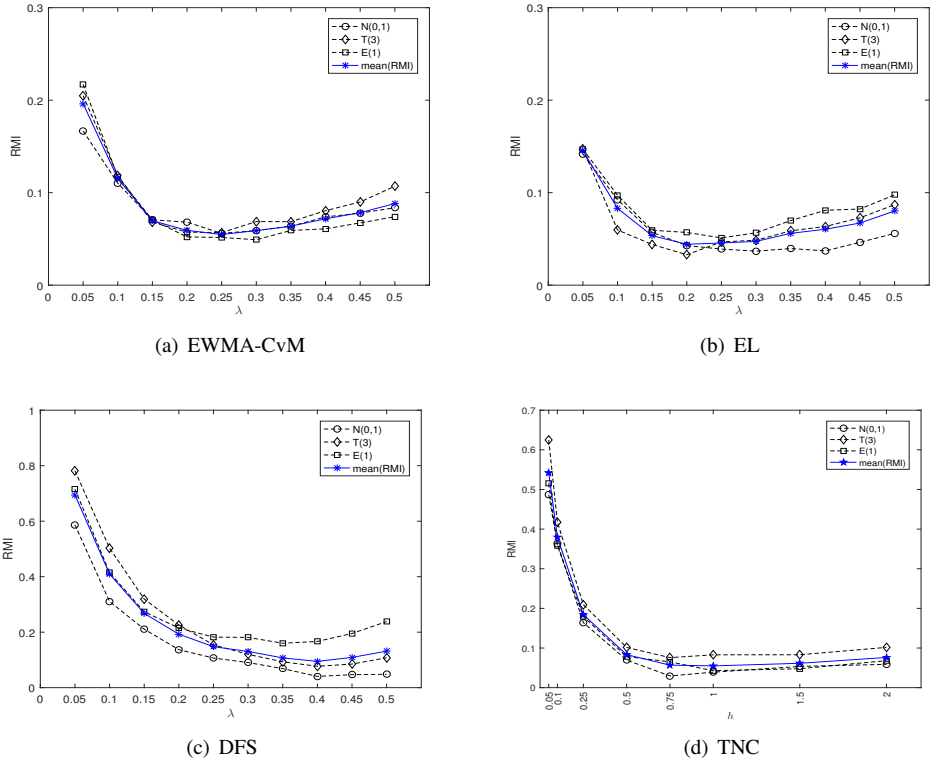

(a) EWMA-CvM (b) EL

(c) DFS (d) TNC

Figure 3: Optimal parameter selection based on RMI for the EWMA-CvM, EL, DFS and TNC schemes when $m = 100, n = 5$ and $\mathrm{MRL}_0 = 250$.

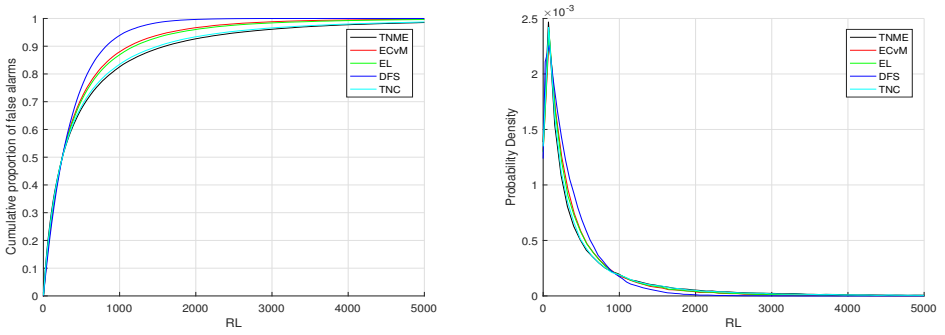

(a) Cumulative proportion (b) Probability density

Figure 4: Probability density and cumulative proportions of false alarm.

We explore an extensive array of OOC "micro" scenarios, ranging from small to large shifts in one, two, or all of the three parameters. It is essential to highlight that the comparisons are based exclusively on the optimal values of λ (or h) for all competing methods. Figure 5 presents the OOC MRL_1 performance of the five competing monitoring techniques for detecting isolated shifts in process location, scale, and shape, respectively. With a fixed IC $\mathrm{MRL}_0 = 250$, a notable observation from the comparative results is that the proposed TNME competes effectively with ECvM and EL schemes, consistently demonstrating superior detection performance for most OOC situations, barring a few exceptions. The TNME scheme displays significantly better detection ability of the location and shape shifts. This observation aligns with the substantial location shift identification capability of the S_t statistic and its substantial correlation with the W_t statistic. Consequently, the combined test statistic M_t outperforms the L_t statistic when detecting location and shape shifts. The finding aligns well with the findings in Kössler and Mukherjee (2020). For monitoring the scale shifts, it is interesting to find that the DFS chart has a significantly better performance than other competitors. It is also worth noting that the ECvM, EL and DFS schemes display MRL-biasedness (MB) for small shifts in the shape parameter, such as $(\delta = 0, \epsilon' = 1, \varrho' = 1.1)$, where the MRL_1 value exceeds the MRL_0.

The TNME and the TNC schemes exhibit somewaht similarities in their performance for detecting isolated shifts. But it becomes evident that the TNME scheme holds a distinct advantage, especially when it comes to detecting shifts involving two or three parameters, such as location-shape, scale-shape, or shifts across all three parameters. Therefore, we can drown the conclusion that the proposed TNME method offers a more comprehensive monitoring effect, particularly in complex industrial applications where multiple aspects of a process need monitoring simultaneously. Significantly, the TNME charting scheme not only excels in identifying more complex shifts but also offers enhanced capabilities during the diagnostic phase, providing a more robust tool for comprehensive monitoring and analysis.

We present the simulation results in Table 4 when considering the OOC cases with various shifts in two parameters. For detecting the location-sale and the scale-shape shifts, the DFS scheme has a better performance for monitoring the N(0, 1) and T(3) distributions, and the TNME scheme performs the best for monitoring the E(1) distribution. For detecting the location-shape shifts, the superiority of the DFS scheme over other schemes becomes evident. We must emphasise that the DFS scheme assumes that the process c.d.f. is fully known or can be accurately estimated. However, in most scenarios, the TNME scheme remains the preferred choice when limited data is available. The same conclusion applies to cases where all three parameters experience shifts, as shown in Table 5. The proposed TNME scheme performs better for detecting large shifts than the DFS scheme. Overall, the TNME control chart has substantial advantages compared to existing control charts, consistently displaying superior performance across various scenarios.

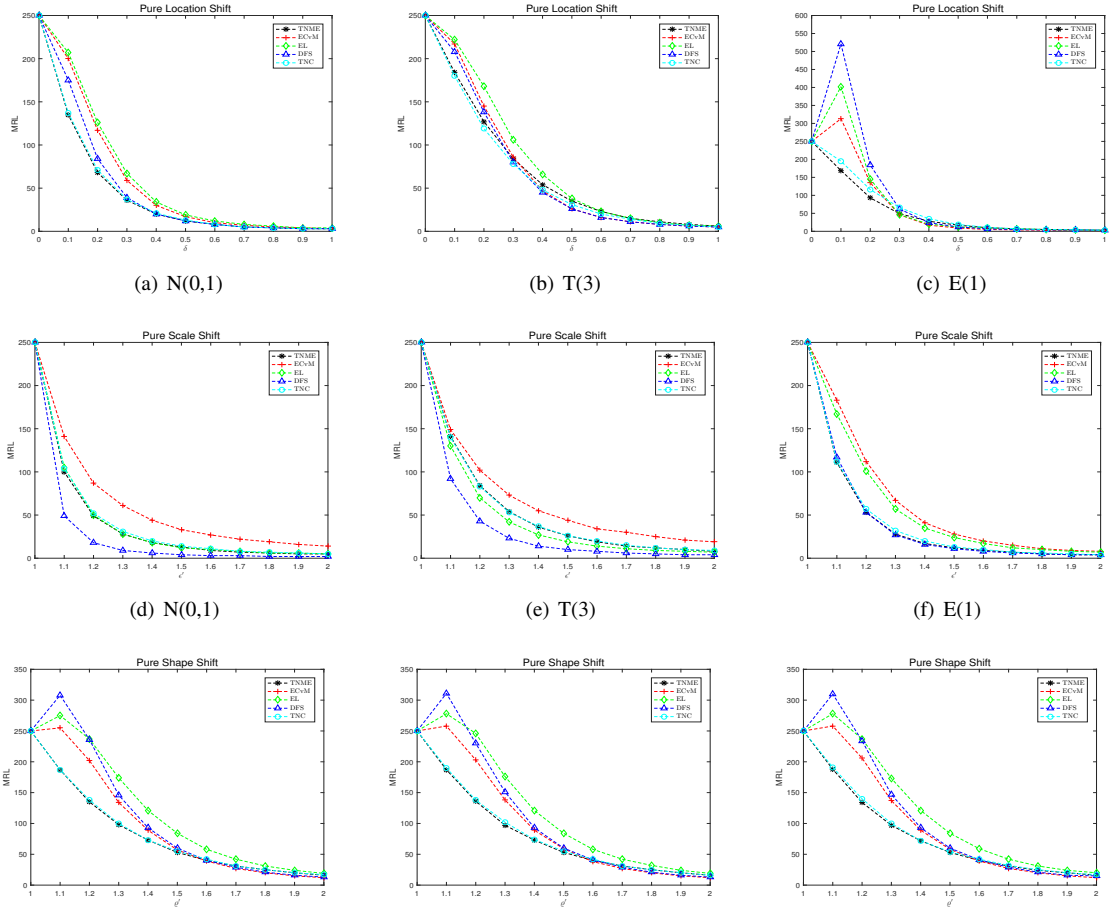

(a) N(0,1) (b) T(3) (c) E(1)

(d) N(0,1) (e) T(3) (f) E(1)

(g) N(0,1) (h) T(3) (i) E(1)

Figure 5: OOC MRL_1 simulation values for pure shifts in the process location, scale and shape when target $MRL_0 = 250$, $m = 100$ and $n = 5$.

Table 3
OOC MRL_1 simulation values of the TNME scheme when target $MRL_0 = 250$, $\lambda = 0.1$, $m \in \{100, 300\}$ and $n \in \{5, 10\}$.

$(\delta, \epsilon', \varrho')$	$m = 100$, $n = 5$				$m = 100$, $n = 10$				$m = 300$, $n = 5$				$m = 300$, $n = 10$			
N(0, 1)	0.05	0.1	0.3	0.5	0.05	0.1	0.3	0.5	0.05	0.1	0.3	0.5	0.05	0.1	0.3	0.5
(0.2, 1, 1)	61	62	68	73	44	47	59	65	52	54	64	69	36	26	46	50
(0, 1.2, 1)	39	41	49	54	33	34	43	47	33	35	44	49	26	29	34	37
(0, 1, 1.6)	29	30	40	48	14	14	18	25	27	30	41	48	13	13	17	23
(0.2, 1.2, 1)	19	19	21	23	15	14	16	18	16	15	18	20	11	9	12	13
(0, 1.2, 1.2)	26	25	28	31	20	20	23	27	21	21	25	28	15	12	17	19
(0.2, 1, 1.2)	27	27	32	38	15	15	19	23	24	25	32	36	13	11	16	20
(0.2, 1.2, 1.2)	12	11	12	13	8	7	8	8	10	9	11	12	7	5	6	7
(0.2, 1.2, 1.4)	8	7	7	8	5	5	5	5	7	7	7	8	4	3	4	4
(0.2, 1.2, 1.6)	6	5	5	6	4	3	3	3	5	5	5	6	3	3	3	3
(0.4, 1.4, 1.2)	5	4	4	4	3	3	3	3	4	4	4	4	3	2	2	2
(0.4, 1.4, 1.4)	4	3	3	3	2	2	2	2	3	3	3	3	2	2	2	2
(0.4, 1.4, 1.6)	3	3	2	2	2	2	2	2	3	2	2	2	2	2	1	1
(0.6, 1.2, 1.2)	4	4	4	4	3	2	2	2	4	3	3	3	2	2	2	2
(0.6, 1.4, 1.2)	3	3	3	3	2	2	2	2	3	3	3	3	2	2	2	2
(0.6, 1.6, 1.2)	3	3	2	2	2	2	2	2	2	2	2	2	2	1	1	1
T(3)	0.05	0.1	0.3	0.5	0.05	0.1	0.3	0.5	0.05	0.1	0.3	0.5	0.05	0.1	0.3	0.5
(0.2, 1, 1)	118	120	127	130	87	92	110	118	106	111	123	131	73	79	96	101
(0, 1.2, 1)	66	70	84	94	54	59	74	82	59	65	85	91	45	49	64	73
(0, 1, 1.6)	39	31	40	47	14	14	19	25	27	30	41	48	13	13	17	22
(0.2, 1.2, 1)	40	41	49	54	29	31	38	43	35	36	47	52	25	25	31	36
(0, 1.2, 1.2)	42	42	48	52	32	33	40	45	35	36	45	51	25	25	32	36
(0.2, 1, 1.2)	43	47	60	66	22	23	32	41	41	45	60	67	20	21	30	37
(0.2, 1.2, 1.2)	21	21	25	28	14	13	15	19	19	19	24	29	12	11	13	15
(0.2, 1.2, 1.4)	13	12	14	17	8	7	7	9	12	12	14	17	7	6	7	8
(0.2, 1.2, 1.6)	9	8	9	11	5	5	5	5	8	8	9	11	5	4	4	5
(0.4, 1.4, 1.2)	9	8	9	10	6	5	5	5	8	8	9	10	5	5	5	5
(0.4, 1.4, 1.4)	6	6	6	6	4	4	3	3	6	5	6	6	3	3	3	3
(0.4, 1.4, 1.6)	5	4	4	5	3	3	2	2	4	4	4	5	3	2	2	2
(0.6, 1.2, 1.2)	8	7	8	9	5	4	4	4	7	7	8	10	4	4	4	4
(0.6, 1.4, 1.2)	6	6	6	6	4	4	3	3	6	5	6	7	4	3	3	3
(0.6, 1.6, 1.2)	5	5	5	5	3	3	3	3	5	5	5	5	3	3	3	3
E(1)	0.05	0.1	0.3	0.5	0.05	0.1	0.3	0.5	0.05	0.1	0.3	0.5	0.05	0.1	0.3	0.5
(0.2, 1, 1)	58	67	93	105	22	23	40	55	66	78	101	108	23	26	45	59
(0, 1.2, 1)	47	48	53	57	39	40	48	52	38	39	46	51	29	29	35	39
(0, 1, 1.6)	29	30	40	47	14	14	19	25	27	30	41	47	13	13	17	23
(0.2, 1.2, 1)	20	19	23	27	10	10	12	15	18	18	22	25	9	9	11	13
(0, 1.2, 1.2)	23	23	26	30	15	14	17	20	20	20	24	28	12	12	14	16
(0.2, 1, 1.2)	28	31	47	55	12	11	16	24	29	33	49	56	11	11	17	25
(0.2, 1.2, 1.2)	11	11	12	15	6	5	6	7	10	10	12	14	5	5	5	6
(0.2, 1.2, 1.4)	8	7	8	9	4	4	4	4	7	7	8	9	4	4	3	4
(0.2, 1.2, 1.6)	6	5	5	6	3	3	3	3	6	5	6	7	3	3	3	3
(0.4, 1.4, 1.2)	4	4	4	4	3	2	2	2	4	4	4	4	2	2	2	2
(0.4, 1.4, 1.4)	3	3	3	3	2	2	2	2	3	3	3	3	2	2	2	2
(0.4, 1.4, 1.6)	3	3	2	2	2	2	1	1	3	3	2	3	2	2	1	1
(0.6, 1.2, 1.2)	4	4	4	4	2	2	2	2	4	4	4	5	2	2	2	2
(0.6, 1.4, 1.2)	3	3	3	3	2	2	2	1	3	3	3	3	2	2	1	1
(0.6, 1.6, 1.2)	3	2	2	2	2	1	1	1	2	2	2	2	1	1	1	1

Table 4
OOC MRL_1 simulation values for the shift in process location-scale, scale-shape and location-shape when target $\mathrm{MRL}_0 = 250$, $m = 100$ and $n = 5$.

				N(0,1)					T(3)					E(1)				
Location-scale	δ	ϵ'	ϱ'	TNME	ECvM	EL	DFS	TNC	TNME	ECvM	EL	DFS	TNC	TNME	ECvM	EL	DFS	TNC
	0.2	1.2	1	21	58	36	14	24	49	74	55	32	46	23	34	43	26	27
	0.2	1.4	1	10	33	15	5	12	24	45	24	13	23	9	14	18	10	11
	0.2	1.6	1	7	23	9	3	7	14	30	13	7	14	6	9	10	6	6
	0.2	1.8	1	5	16	6	2	5	9	22	9	5	10	4	6	7	4	4
	0.4	1.4	1	6	18	10	4	7	15	26	17	10	15	6	6	8	6	6
	0.6	1.4	1	4	10	7	3	4	9	14	11	7	9	4	3	5	4	4
	0.8	1.4	1	3	6	5	3	3	6	9	7	5	6	3	2	3	3	2
	1	1.4	1	2	4	3	2	2	4	6	5	4	4	2	2	2	2	2
Scale-shape	δ	ϵ'	ϱ'	TNME	ECvM	EL	DFS	TNC	TNME	ECvM	EL	DFS	TNC	TNME	ECvM	EL	DFS	TNC
	0	1.2	1.2	28	72	54	22	32	48	86	74	48	48	26	47	52	28	29
	0	1.2	1.4	17	39	34	16	19	27	43	46	28	28	15	20	26	15	16
	0	1.2	1.6	11	20	21	11	12	16	22	25	16	17	10	11	15	9	10
	0	1.2	1.8	8	12	13	8	9	11	13	16	10	11	7	8	10	7	7
	0	1.4	1.2	12	37	19	7	13	23	47	29	17	23	10	18	18	10	11
	0	1.6	1.2	7	24	10	4	8	13	30	16	9	14	5	9	9	5	6
	0	1.8	1.2	5	17	7	3	5	9	22	10	6	9	4	6	6	4	4
	0	2	1.2	4	13	5	2	4	6	17	7	4	7	3	5	5	3	3
Location-shape	δ	ϵ'	ϱ'	TNME	ECvM	EL	DFS	TNC	TNME	ECvM	EL	DFS	TNC	TNME	ECvM	EL	DFS	TNC
	0.2	1	1.2	32	44	57	35	35	60	59	84	60	55	47	40	55	48	51
	0.2	1	1.4	18	19	26	17	19	30	24	38	25	30	24	17	27	20	26
	0.2	1	1.6	11	10	15	10	12	17	12	20	14	17	15	10	16	11	15
	0.2	1	1.8	8	7	10	7	8	11	8	12	9	11	10	7	10	8	10
	0.4	1	1.2	11	12	16	10	11	24	18	27	19	23	16	9	13	11	17
	0.6	1	1.2	5	6	7	5	5	11	8	11	8	10	7	4	7	5	7
	0.8	1	1.2	3	3	4	3	3	6	5	6	5	5	4	3	4	4	4
	1	1	1.2	2	2	3	2	2	4	3	4	4	4	3	2	3	3	2

Table 5
OOC MRL_1 simulation values for the shift in process location-scale-shape when target $MRL_0 = 250$, $m = 100$ and $n = 5$.

				N(0,1)					T(3)					E(1)				
Location-scale-shape	δ	ϵ'	ϕ'	TNME	ECvM	EL	DFS	TNC	TNME	ECvM	EL	DFS	TNC	TNME	ECvM	EL	DFS	TNC
	0.2	1.2	1.2	12	27	23	11	13	25	36	36	23	24	12	14	19	12	14
	0.2	1.2	1.4	7	14	13	7	8	14	17	20	13	14	8	8	10	7	8
	0.2	1.2	1.6	5	8	9	6	6	9	10	12	8	9	6	5	7	5	6
	0.2	1.2	1.8	4	6	6	4	4	6	7	8	6	6	4	4	5	4	4
	0.2	1.4	1.2	7	18	12	5	7	14	24	18	11	14	6	7	9	6	6
	0.2	1.4	1.4	5	11	8	4	5	9	13	12	8	9	4	5	6	4	4
	0.2	1.4	1.6	4	7	6	4	4	6	8	8	6	6	3	4	4	4	3
	0.2	1.4	1.8	3	5	5	3	3	5	6	6	5	4	3	3	4	3	3
	0.2	1.6	1.2	5	14	8	3	5	9	19	11	7	9	4	5	6	4	4
	0.2	1.6	1.4	3	9	6	3	4	6	11	8	6	6	3	4	4	3	3
	0.2	1.6	1.6	3	6	5	3	3	4	7	6	5	5	2	3	3	3	2
	0.2	1.6	1.8	2	4	4	2	2	4	5	5	4	4	2	2	3	2	2
	0.2	1.8	1.2	4	11	6	2	4	7	15	8	5	7	3	4	4	3	3
	0.2	1.8	1.4	3	7	5	2	3	5	9	6	4	5	2	3	3	3	2
	0.2	1.8	1.6	2	5	4	2	2	4	6	5	4	4	2	2	3	2	2
	0.2	1.8	1.8	2	4	3	2	2	3	5	4	3	3	2	2	2	2	2
	0.4	1.2	1.2	6	11	10	6	6	13	15	17	11	13	6	5	8	6	7
	0.4	1.2	1.4	4	7	7	4	4	8	8	10	7	8	4	4	6	4	5
	0.4	1.2	1.6	3	4	5	4	3	6	6	7	5	5	4	3	4	4	3
	0.4	1.2	1.8	3	3	4	3	3	4	4	5	4	4	3	3	3	3	3
	0.4	1.4	1.2	4	10	7	4	5	9	13	11	8	8	4	4	5	4	4
	0.4	1.4	1.4	3	6	5	3	3	6	8	7	6	6	3	3	4	3	3
	0.4	1.4	1.6	2	4	4	3	3	4	5	5	4	4	2	3	3	3	2
	0.4	1.4	1.8	2	3	3	2	2	3	4	4	4	3	2	2	3	2	2
	0.4	1.6	1.2	3	9	6	3	4	6	11	8	6	6	3	3	4	3	3
	0.4	1.6	1.4	2	6	4	2	3	5	7	6	4	4	2	3	3	3	2
	0.4	1.6	1.6	2	4	3	2	2	3	5	5	4	3	2	2	2	2	2
	0.4	1.6	1.8	2	3	3	2	2	3	4	4	3	3	2	2	2	2	2
	0.4	1.8	1.2	3	8	5	2	3	5	10	6	4	5	2	3	3	3	2
	0.4	1.8	1.4	2	5	4	2	2	4	6	5	4	4	2	2	2	2	2
	0.4	1.8	1.6	2	4	3	2	2	3	5	4	3	3	2	2	2	2	2
	0.4	1.8	1.8	2	3	3	2	2	2	3	3	3	2	1	2	2	2	1
	0.6	1.2	1.2	3	6	5	4	4	8	8	9	7	7	4	3	4	4	4
	0.6	1.2	1.4	3	4	4	3	3	5	5	6	5	5	3	3	3	3	3
	0.6	1.2	1.6	2	3	3	3	2	4	4	4	4	4	3	2	3	3	2
	0.6	1.2	1.8	2	2	3	2	2	3	3	3	3	3	2	2	2	3	2
	0.6	1.4	1.2	3	6	6	3	3	6	8	7	5	6	3	3	3	3	3
	0.6	1.4	1.4	2	4	4	2	2	4	5	5	4	4	2	2	3	3	2
	0.6	1.4	1.6	2	3	3	2	2	3	4	4	3	3	2	2	2	2	2
	0.6	1.4	1.8	2	2	3	2	2	3	3	3	3	2	2	2	2	2	2
	0.6	1.6	1.2	2	6	5	2	3	5	7	6	4	5	2	2	3	2	2
	0.6	1.6	1.4	2	4	4	2	2	3	5	4	4	3	2	2	2	2	2
	0.6	1.6	1.6	2	3	3	2	2	3	4	3	3	3	2	2	2	2	2
	0.6	1.6	1.8	1	2	2	2	2	2	3	3	3	2	1	2	2	2	1
	0.6	1.8	1.2	2	5	4	2	2	4	7	5	4	4	2	2	2	2	2
	0.6	1.8	1.4	2	4	3	2	2	3	5	4	3	3	1	2	2	2	2
	0.6	1.8	1.6	2	3	3	2	2	2	3	3	3	2	1	2	2	2	1
	0.6	1.8	1.8	1	2	2	1	1	2	3	3	2	2	1	2	2	2	1
	0.8	1.2	1.2	2	4	4	3	2	5	5	5	5	5	3	2	3	3	3
	0.8	1.2	1.4	2	3	3	2	2	4	4	4	4	3	2	2	2	3	2
	0.8	1.2	1.6	2	2	2	2	2	3	3	3	3	3	2	2	2	2	2
	0.8	1.2	1.8	1	2	2	2	1	2	2	3	3	2	2	2	2	2	2
	0.8	1.4	1.2	2	4	4	2	2	4	5	5	4	4	2	2	2	2	2
	0.8	1.4	1.4	2	3	3	2	2	3	4	4	3	3	2	2	2	2	2
	0.8	1.4	1.6	1	2	2	2	2	2	3	3	3	2	2	2	2	2	1
	0.8	1.4	1.8	1	2	2	2	1	2	2	2	2	2	1	2	2	2	1
	0.8	1.6	1.2	2	4	3	2	2	4	5	4	3	3	2	2	2	2	2
	0.8	1.6	1.4	2	3	3	2	2	3	4	3	3	3	2	2	2	2	1
	0.8	1.6	1.6	1	2	2	2	1	2	3	3	3	2	1	2	2	2	1
	0.8	1.6	1.8	1	2	2	1	1	2	2	2	2	2	1	1	1	2	1
	0.8	1.8	1.2	2	4	3	2	2	3	5	4	3	3	1	2	2	2	1
	0.8	1.8	1.4	2	3	2	2	2	2	4	3	3	2	1	2	2	2	1
	0.8	1.8	1.6	1	2	2	1	1	2	3	3	2	2	1	1	1	2	1
	0.8	1.8	1.8	1	2	2	1	1	2	2	2	2	2	1	1	1	1	1

5. Examples analysis

This part demonstrates the implementation of the TNME scheme using two real-data examples reported in Montgomery (2012). We commence by examining an illustration rooted in the renowned piston ring statistics. Subsequently, we explore a second example involving monitoring flow width in semiconductor manufacturing.

5.1. Forging process monitoring

In this subsection, we hope to establish a nonparametric chart for monitoring the inner diameters of the rings in a forging process. Here, we use the proposed TNME chart for monitoring this operation. The Phase-I data in Montgomery (2012), is made up of 125 IC reference observations, and the Phase-II data in Montgomery (2012) consists of 15 test samples each of size 5. Therefore, when $m = 125$, $n = 5$ and target $\mathrm{MRL}_0 = 250$, we obtain, using Monte Carlo methods, the optimal $\lambda = 0.3$ and the corresponding UCL $= 4.236$ for the TNME chart, optimal $\lambda = 0.25$ and UCL $= 1.405$ for the ECvM chart, optimal $\lambda = 0.2$ and UCL $= 4.139$ for the EL chart, optimal $\lambda = 0.4$ and UCL $= 3.6$ for the DFS chart, optimal $h = 1$ and UCL $= 15.28$ for the TNC chart.

The charting statistics M_t, E_t, Z_t, R_t and Q_t are depicted in Figure 6. The initial OOC signal is observed at the 12^{th} sample for the TNME, ECvM, DFS and TNC charts, and at the 13^{th} sample for the EL chart. It's important to highlight that both the ECvM and DFS approaches lack the ability to pinpoint the primary contributors-be it location, scale, or shape-in generating a signal. This characteristic of the the bi-aspect and tri-aspect schemes simplifies the diagnostic verification process in practical applications when compared to its counterparts. If the objective is to pinpoint the predominant factor (location, scale, or shape) responsible for this signal, the follow-up procedure of the TNME charting scheme proves to be the simplest approach. This approach only requires scrutinizing the values of $Q_{W,t}$, $Q_{A,t}$, and $Q_{S,t}$ against the UCL. Upon examination, it becomes evident that the statistic associated with $Q_{S,t}$ corresponds to the contributing factor behind the signal. This observation signifies a shift in the process shape.

5.2. Hard-bake process monitoring

In this subsection, we consider a realistic dataset associated with semiconductor manufacturing, as introduced in Montgomery (2012). In semiconductor production, photolithography plays a crucial role. This intricate process involves coating a silicon wafer with a photosensitive substance known as photoresist. Typically, high-intensity ultraviolet light is employed to expose the circuit layout onto the resist. Subsequent to this step, the extraneous resist material is eradicated during the development process. To transfer the resist pattern onto the substrate, two distinct methods can be employed: wet etching and dry etching. Wet etching employs liquid chemicals or etchants, while dry etching, like plasma etching, hinges on plasmas or etchant gases. Following this step, a hard-bake technique is often employed to enhance adhesion and etch resistance. Notably, in hard bake procedures, the flow width of the resist serves as a critical quality indicator. Therefore, the establishment of charting schemes for the vigilance of resist flow width becomes essential to detect any atypical alterations in the process's underlying location, scale, or shape parameters.

In Phase-I, we use the 125 observations in Montgomery (2012) as the IC reference data. Thus, in this context, we have $m = 125$. In Phase-II, we monitor 20 test samples each of size $n = 5$. For $m = 125$, $n = 5$ and target $\mathrm{MRL}_0 = 250$, we shall employ the same charting scheme as described in the previous example for monitoring purposes. We present the plotting statistics $Q_{W,t}$, $Q_{A,t}$ and $Q_{S,t}$ of the TNME, ECvM, EL and TNC charts, respectively, in Figure 7.

The initial OOC signal is observed at the 15^{th} sample for the TNME chart. In contrast, the remaining three charts breach the UCL for the first time at the 16^{th} sample. Concerning the TNME chart, beyond detecting the signal at the 15^{th} sample, a crucial point of interest pertains to identifying the specific factor (location, scale, or shape) accountable for this signal. Based on our meticulous analysis, we can deduce that the statistics tied to the $Q_{S,t}$ component highlight a dominant shift in the process shape, thereby underscoring its primary role as the driving cause behind the observed signal.

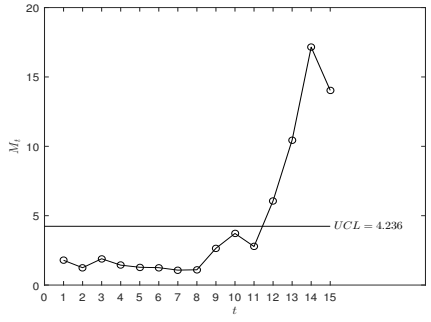

(a) TNME

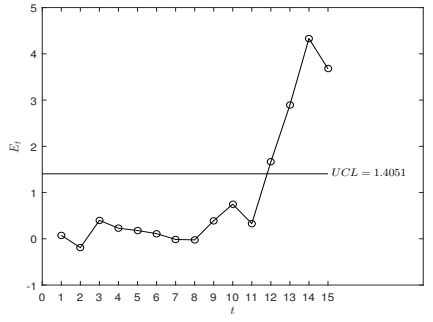

(b) ECvM

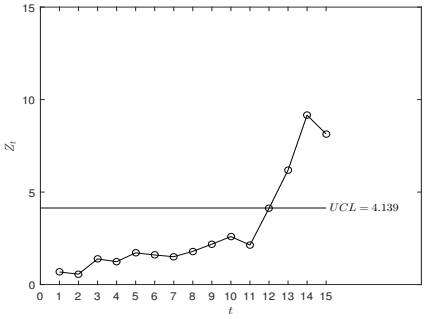

(c) EL

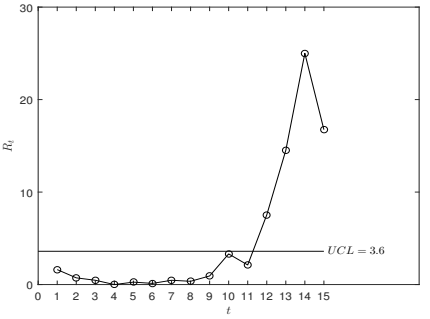

(d) DFS

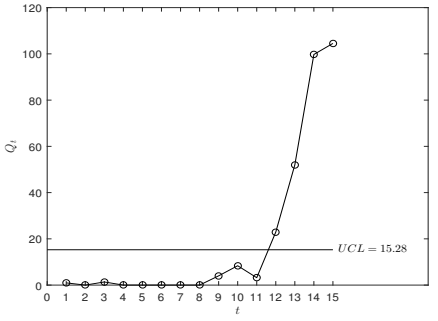

(e) TNC

Figure 6: TNME, ECvM, EL, DFS and TNC schemes for monitoring the forging process.

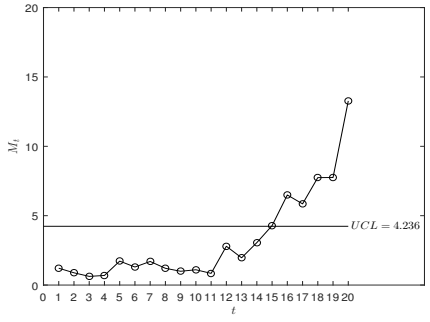

(a) TNME

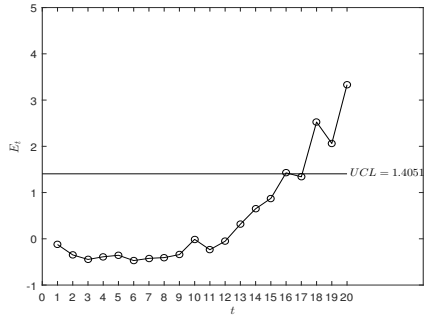

(b) ECvM

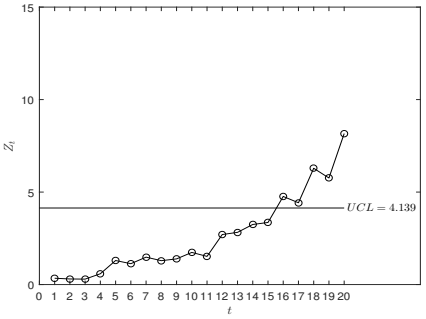

(c) EL

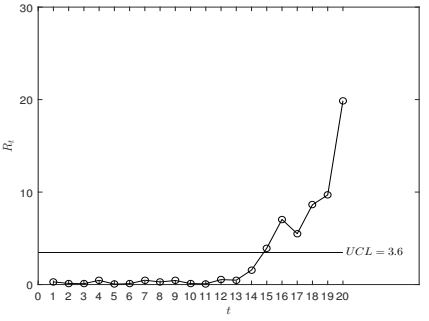

(d) DFS

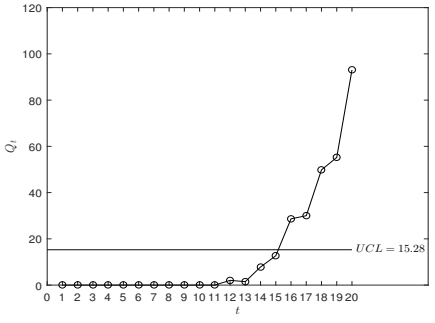

(e) TNC

Figure 7: TNME, ECvM, EL, DFS and TNC schemes for monitoring hard-bake process.

6. Concluding remarks

This paper introduces a novel nonparametric Max-EWMA scheme that employs a tri-aspect statistic to identify alterations in the location, scale, and shape parameters, both individually and in combination. The proposed TNME scheme integrates standardized WRS statistics for location, standardized AB statistics for scale, and standardized SA statistics for shape. Our approach's implementation strategy relies on the MRL measure, with its robustness validated across various distributions through Monte Carlo simulations. A central focus of this paper revolves around determining the optimal λ parameter for the proposed Max-EWMA chart. This parameter choice facilitates the detection of a broad spectrum of unknown location-scale-shape shifts. Furthermore, we conduct a comparative analysis by evaluating the performance of our proposed scheme against other contenders using the MRL metric. The results underscore our approach's remarkable competitiveness and extensive applicability in identifying shifts in location, scale, or shape parameters. It outperforms existing bi-aspect or tri-aspect schemes like CCvM, EL, DFS and TNC schemes.

As an avenue for further research, we suggest exploring other combinations of statistics, particularly various orthogonal statistics, as an alternative to our proposed scheme. Additionally, there is room to explore an adaptive EWMA scheme that concurrently monitors unspecified shifts in location, scale, and shape. This can be achieved by employing data-dependent λ values assigned to the three constituent statistics.

Disclosure statement

No potential conflict of interest was reported by the authors.

Acknowledgements

This work is supported by the National Nature Science Foundation of China [grant number 72101123]; Natural Science Foundation of Jiangsu Province [grant number BK20200750]; Philosophy and Social Sciences Foundation of Jiangsu Universities [grant number 2020SJA0090]; Nanjing Science and Technology Innovation Project for Overseas Educators [grant number NJKCZYZZ2022-08].

References

Abid, M., Nazir, H.Z., Riaz, M., Lin, Z., 2017. An efficient nonparametric EWMA Wilcoxon signed-rank chart for monitoring location. Quality and Reliability Engineering International 33, 669–685.

Alevizakos, V., Chatterjee, K., Koukouvinos, C., 2021. Nonparametric triple exponentially weighted moving average signed-rank control chart for monitoring shifts in the process location. Quality and Reliability Engineering International 37, 2622–2645.

Ali, S., Akram, M.F., Shah, I., 2022. Max-EWMA chart using beta and simplex distributions for time and magnitude monitoring. Mathematical Problems in Engineering Doi:10.1155/2022/7306775.

Almanjahie, I.M., Rasheed, Z., Khan, M., Anwar, S.M., Cheema, A.N., 2023. Ranked-set sampling based distribution free control chart with application in CSTR process. CMES-Computer Modeling in Engineering & Sciences 135.

Anwar, S.M., Aslam, M., Zaman, B., Riaz, M., 2021. Mixed memory control chart based on auxiliary information for simultaneously monitoring of process parameters: An application in glass field. Computers & Industrial Engineering 156, 107284.

Capizzi, G., Masarotto, G., 2017. Phase i distribution-free analysis of multivariate data. Technometrics 59, 484–495.

Castagliola, P., Tran, K.P., Celano, G., Maravelakis, P.E., 2020. The Shewhart sign chart with ties: Performance and alternatives, in: Distribution-Free Methods for Statistical Process Monitoring and Control. Springer, pp. 107–136.

Chakraborti, S., Van der Laan, P., Van de Wiel, M., 2004. A class of distribution-free control charts. Journal of the Royal Statistical Society: Series C (Applied Statistics) 53, 443–462.

Chan, K.M., Chong, Z.L., Mukherjee, A., 2022. Exponentially weighted moving average Lepage-type schemes based on the lower-order percentile of the run-length metrics and their use in mon- itoring time-occupancy in Google applications. Quality Technology & Quantitative Management doi:10.1080/16843703.2022.2132452.

Chan, K.M., Mukherjee, A., Chong, Z.L., Lee, H.C., 2021. Distribution-free double exponentially and homogeneously weighted moving average Lepage schemes with an application in monitoring exit rate. Computers & Industrial Engineering 161, 107370.

Chong, Z.L., Mukherjee, A., Khoo, M.B., 2020. Some simplified Shewhart-type distribution-free joint monitoring schemes and its application in monitoring drinking water turbidity. Quality Engineering 32, 91–110.

Chong, Z.L., Tan, K.L., Khoo, M.B., Teoh, W.L., Castagliola, P., 2022. Optimal designs of the exponentially weighted moving average (EWMA) median chart for known and estimated parameters based on median run length. Communications in Statistics-Simulation and Computation 51, 3660–3684.

Chowdhury, S., Mukherjee, A., Chakraborti, S., 2015. Distribution-free Phase II CUSUM control chart for joint monitoring of location and scale. Quality and Reliability Engineering International 31, 135–151.

Das, N., Bhattacharya, A., 2008. A new non-parametric control chart for controlling variability. Quality Technology & Quantitative Management 5, 351–361.

Ding, D., Li, J., Tsung, F., Li, Y., 2023. A Phase II score-based distribution-free method for jointly monitoring location and scale. Quality and Reliability Engineering International .

Erfanian, M., Sadeghpour Gildeh, B., Reza Azarpazhooh, M., 2021. A new approach for monitoring healthcare performance using generalized additive profiles. Journal of Statistical Computation and Simulation 91, 167–179.

Graham, M.A., Mukherjee, A., Chakraborti, S., 2012. Distribution-free exponentially weighted moving average control charts for monitoring unknown location. Computational Statistics & Data Analysis 56, 2539–2561.

Graham, M.A., Mukherjee, A., Chakraborti, S., 2017. Design and implementation issues for a class of distribution-free Phase II EWMA exceedance control charts. International Journal of Production Research 55, 2397–2430.

Han, D., Tsung, F., 2006. A reference-free cuscore chart for dynamic mean change detection and a unified framework for charting performance comparison. Publications of the American Statistical Association 101, 368–386.

Haq, A., 2017. A new nonparametric EWMA control chart for monitoring process variability. Quality and Reliability Engineering International 33, 1499–1512.

Javaid, A., Noor-ul Amin, M., Hanif, M., 2020. Performance of Max-EWMA control chart for joint monitoring of mean and variance with measurement error. Communications in Statistics-Simulation and Computation doi:10.1080/03610918.2020.1842886.

Keshavarz, M., Asadzadeh, S., Niaki, S.T.A., 2021. Risk-adjusted frailty-based CUSUM control chart for Phase I monitoring of patients' lifetime. Journal of Statistical Computation and Simulation 91, 334–352.

Kössler, W., Mukherjee, A., 2020. Distribution-free simultaneous tests for location–scale and Lehmann alternative in two-sample problem. Biometrical Journal 62, 99–123.

Li, C., Mukherjee, A., Marozzi, M., 2020. A new distribution-free Phase-I procedure for bi-aspect monitoring based on the multi-sample Cucconi statistic. Computers & Industrial Engineering 149, 106760.

Li, C., Mukherjee, A., Su, Q., 2019. A distribution-free Phase I monitoring scheme for subgroup location and scale based on the multi-sample lepage statistic. Computers & Industrial Engineering 129, 259–273.

Li, C., Mukherjee, A., Su, Q., Xie, M., 2016. Optimal design of a distribution-free quality control scheme for cost-efficient monitoring of unknown location. International Journal of Production Research 54, 7259–7273.

Liang, W., Mukherjee, A., Xiang, D., Xu, Z., 2022. A new nonparametric adaptive EWMA procedures for monitoring location and scale shifts via weighted Cucconi statistic. Computers & Industrial Engineering 170, 108321.

Malela-Majika, J.C., 2021. New distribution-free memory-type control charts based on the Wilcoxon rank-sum statistic. Quality Technology & Quantitative Management 18, 135–155.

Malela-Majika, J.C., Rapoo, E., 2017. Distribution-free mixed cumulative sum-exponentially weighted moving average control charts for detecting mean shifts. Quality and Reliability Engineering International 33, 1983–2002.

Montgomery, D.C., 2012. Introduction to statistical quality control. John Wiley & Sons.

Mukherjee, A., Chakraborti, S., 2012. A distribution-free control chart for the joint monitoring of location and scale. Quality and Reliability Engineering International 28, 335–352.

Mukherjee, A., Cheng, Y., Gong, M., 2018. A new nonparametric scheme for simultaneous monitoring of bivariate processes and its application in monitoring service quality. Quality Technology & Quantitative Management 15, 143–156.

Mukherjee, A., Marozzi, M., 2021. Nonparametric Phase-II control charts for monitoring high-dimensional processes with unknown parameters. Journal of Quality Technology 54, 44–64.

Mukherjee, A., Qiu, P., Marozzi, M., 2021. A comprehensive distribution-free scheme for tri-aspect surveillance of complex processes. Applied Stochastic Models in Business and Industry 37, 1157–1181.

Mukherjee, A., Sen, R., 2015. Comparisons of Shewhart-type rank based control charts for monitoring location parameters of univariate processes. International Journal of Production Research 53, 4414–4445.

Mukherjee, A., Sen, R., 2018. Optimal design of Shewhart-Lepage type schemes and its application in monitoring service quality. European Journal of Operational Research 266, 147–167.

Noorul-Amin, M., Javaid, A., Hanif, M., Dogu, E., 2022. Performance of maximum EWMA control chart in the presence of measurement error using auxiliary information. Communications in Statistics-Simulation and Computation 51, 5482–5506.

Perdikis, T., Celano, G., Psarakis, S., Castagliola, P., 2023. An exponentially weighted moving average control chart based on signed ranks for finite horizon processes. Quality Engineering 35, 290–303.

Qiu, P., 2013. Introduction to statistical process control. CRC press.

Qiu, P., 2018. Some perspectives on nonparametric statistical process control. Journal of Quality Technology 50, 49–65.

Rasheed, Z., Khan, M., Abiodun, N.L., Anwar, S.M., Khalaf, G., Abbasi, S.A., 2022. Improved nonparametric control chart based on ranked set sampling with application of chemical data modelling. Mathematical Problems in Engineering 2022.

Rasheed, Z., Zhang, H., Arslan, M., Zaman, B., Anwar, S.M., Abid, M., Abbasi, S.A., 2021. An efficient robust nonparametric triple EWMA Wilcoxon signed-rank control chart for process location. Mathematical Problems in Engineering 2021, 1–28.

Sanusi, R.A., Teh, S.Y., Khoo, M.B., 2020. Simultaneous monitoring of magnitude and time-between-events data with a Max-EWMA control chart. Computers & Industrial Engineering 142, 106378.

Song, Z., Mukherjee, A., Marozzi, M., Zhang, J., 2020a. A class of distribution-free exponentially weighted moving average schemes for joint monitoring of location and scale parameters, in: Distribution-Free Methods for Statistical Process Monitoring and Control. Springer, pp. 183–217.

Song, Z., Mukherjee, A., Zhang, J., 2020b. An efficient approach of designing distribution-free exponentially weighted moving average schemes with dynamic fast initial response for joint monitoring of location and scale. Journal of Statistical Computation and Simulation 90, 2329–2353.

Suzuki, A., Murakami, H., Mukherjee, A., 2021. Distribution-free Phase-I scheme for location, scale and skewness shifts with an application in monitoring customers' waiting time. Journal of Applied Statistics , 1–21.

Talib, A., Ali, S., Shah, I., 2022. Max-ewma chart for time and magnitude monitoring using exponentially modified gaussian distribution. Quality and Reliability Engineering International 38, 1092–1111.

Tang, A., Castagliola, P., Sun, J., Hu, X., 2019. Optimal design of the adaptive EWMA chart for the mean based on median run length and expected median run length. Quality Technology & Quantitative Management 16, 439–458.

Tang, A., Mukherjee, A., Ma, Y., 2023. An optimally designed distribution-free cusum procedure for tri-aspect surveillance of continuous processes. Quality and Reliability Engineering International .

Teoh, W.L., Chong, J.K., Khoo, M.B., Castagliola, P., Yeong, W.C., 2017. Optimal designs of the variable sample size chart based on median run length and expected median run length. Quality and Reliability Engineering International 33, 121–134.

Teoh, W.L., Lim, J., Khoo, M.B., Chong, Z.L., Yeong, W.C., 2018. Optimal designs of ewma charts for monitoring the coefficient of variation based on median run length and expected median run length. Journal of Testing and Evaluation 47, 459–479.

Wu, S., Castagliola, P., Celano, G., 2021. A distribution-free ewma control chart for monitoring time-between-events-and-amplitude data. Journal of Applied Statistics 48, 434–454.

Wu, Z., Li, Y., Tsung, F., Pan, E., 2023. Real-time monitoring and diagnosis scheme for iot-enabled devices using multivariate spc techniques. IISE Transactions 55, 348–362.

Xiang, D., Gao, S., Li, W., Pu, X., Dou, W., 2019. A new nonparametric monitoring of data streams for changes in location and scale via cucconi statistic. Journal of Nonparametric Statistics 31, 743–760.

Yan, H., Grasso, M., Paynabar, K., Colosimo, B.M., 2022. Real-time detection of clustered events in video-imaging data with applications to additive manufacturing. IISE Transactions 54, 464–480.

You, H., Khoo, M.B., Castagliola, P., Qu, L., 2016. Optimal exponentially weighted moving average charts with estimated parameters based on median run length and expected median run length. International Journal of Production Research 54, 5073–5094.

Zhang, H., Rasheed, Z., Khan, M., Namangale, J.J., Anwar, S.M., Hamid, A., 2022. A distribution-free thwma control chart under ranked set sampling. Mathematical Problems in Engineering 2022.

Zhang, J., Li, E., Li, Z., 2017. A cramér-von mises test-based distribution-free control chart for joint monitoring of location and scale. Computers & Industrial Engineering 110, 484–497.

Zhang, T., He, Z., Zhao, X., Qu, L., 2021. Joint monitoring of post-sales online review processes based on a distribution-free ewma scheme. Computers & Industrial Engineering 158, 107372.

Zhao, C., Lui, C.F., Du, S., Wang, D., Shao, Y., 2023. An earth mover's distance based multivariate generalized likelihood ratio control chart for effective monitoring of 3d point cloud surface. Computers & Industrial Engineering 175, 108911.

Zhou, M., Zhou, Q., Geng, W., 2016. A new nonparametric control chart for monitoring variability. Quality and Reliability Engineering International 32, 2471–2479.